JOURNAL OF CATALYSIS **166,** 44–52 (1997)
ARTICLE NO. CA971497

Platinum–Tin Catalysts Supported on Silica Highly Selective for *n*-Hexane Dehydrogenation

Jordi Llorca,* Narcís Homs,*,[1] José-Luis G. Fierro,† Joaquim Sales,* and Pilar Ramírez de la Piscina*

*Departament de Química Inorgànica, Universitat de Barcelona, Diagonal 647, 08028 Barcelona, Spain; †Instituto de Catálisis y Petroleoquímica, C.S.I.C., Cantoblanco, 28049 Madrid, Spain

Received June 30, 1996; revised October 9, 1996; accepted October 15, 1996

Silica-supported Pt–Sn catalysts were prepared by two-step impregnation from $[PtCl_2(PPh_3)_2]$ and $SnCl_2$ solutions of appropriate concentrations to yield Pt/Sn atomic ratios ranging from 0.2 to 5.0. In these systems, the presence of true Pt–Sn alloys was confirmed by X-ray diffraction, transmission electron microscopy, energy dispersive X-ray analysis and electron nanodiffraction. Pt and PtSn alloy phases were found on catalysts with Pt/Sn > 1, PtSn alloy alone on the catalyst with Pt/Sn = 1 and PtSn and $PtSn_2$ alloys, together with Sn in the catalysts with Pt/Sn < 1. All these catalysts were tested in the skeletal reactions of *n*-hexane at 753 K and atmospheric pressure. The selectivity of Pt changed significantly when alloyed with tin. For Sn-rich compositions a segregation of tin toward the catalyst surface was shown by photoelectron spectroscopy, and high hydrogenolysis selectivity and fast deactivation were observed. In contrast, Pt-rich catalysts, in which a well defined PtSn alloy was observed, were much more stable and exhibited high selectivity to dehydrogenation reaction while maintaining low conversions to benzene and hydrogenolysis products. This selectivity pattern can be interpreted in terms of a change in adsorption properties due to differences in the number of adjacent Pt atoms required for the various reaction pathways.

INTRODUCTION

Supportedbimetallic catalysts based on platinum have been widely studied due to their applications in the reforming process; however, their superior catalytic properties have not been adequately understood, even after 30 years of research (1). Various preparation procedures have been used for supported platinum–tin catalysts, and the goal of many studies has been to relate their structure to their catalytic properties in hydrocarbon reactions (dehydrocyclization, isomerization, hydrogenolysis, etc.) (2–10). Several types of active site have been evidenced and their adsorption and catalytic properties have been determined. However, whether the effects of tin are electronic or geometric and the accurate formulation of platinum–tin entities are still controversial (7, 8, 11, 12).

[1] To whom correspondence should be addressed.

Recently we reported the preparation of a single well-defined PtSn phase supported on silica, with rather large crystal size, using $[PtCl_2(PPh_3)_2]$ and $SnCl_2$ (1 : 1) as precursors (13). This work was undertaken to study the performance of well defined PtSn alloys in hydrocarbon reactions. Here we tailor the preparation of silica-supported Pt–Sn catalysts by changing the $[PtCl_2(PPh_3)_2]/SnCl_2$ ratio used during the impregnation step. We relate the metallic phases in the catalyst with the ratio $[PtCl_2(PPh_3)_2]/SnCl_2$ used in their preparation. The catalysts were characterized by X-ray diffraction (XRD), transmission electron microscopy (TEM), energy dispersive X-ray analysis (EDX), electron nanodiffraction (ED), and X-ray photoelectron spectroscopy (XPS). The behavior of these catalysts in the skeletal reactions of *n*-hexane is reported and related to the different metallic phases present in the catalysts.

EXPERIMENTAL

Preparation of Catalysts

Synthesis of platinum–tin catalysts supported on silica involved the following steps:

(i) The support (Degussa Aerosil-type silica with a BET surface area of 200 $m^2\ g^{-1}$) was partially dehydrated by treatment under high vacuum at 473 K for 16 h.

(ii) Incorporation of platinum was carried out from a methylene chloride solution of *cis*-$[PtCl_2(PPh_3)_2]$ followed by a vacuum treatment at 373 K overnight. All samples were prepared with a 3% platinum loading. The complex *cis*-$[PtCl_2(PPh_3)_2]$ was prepared and characterized according to literature methods (14).

(iii) Incorporation of tin was achieved from an acetone solution of $SnCl_2$ followed by a vacuum treatment at 373 K overnight. The amount of tin introduced in the samples varied from 0.36 to 9% in order to attain Pt/Sn molar ratios from Pt : Sn = 5 : 1 to Pt : Sn = 1 : 5.

(iv) Samples were reduced in a glass reactor at atmospheric pressure in flowing hydrogen (40 ml min^{-1}) at 1.5 K min^{-1} up to 673 K for 16 h. The catalysts obtained are referred to as *a*Pt*b*Sn/SiO_2, where *a*/*b* is the molar

0021-9517/97 $25.00

ratio $[PtCl_2(PPh_3)_2]/SnCl_2$ used in their preparation. Five catalysts have been prepared: $5Pt1Sn/SiO_2$, $2Pt1Sn/SiO_2$, $1Pt1Sn/SiO_2$, $1Pt2Sn/SiO_2$, and $1Pt5Sn/SiO_2$.

For comparative purposes, one catalyst with only platinum (3% loading) in the active phase was prepared from *cis*-$[PtCl_2(PPh_3)_2]$ as reported previously (13), which is referred to as Pt/SiO_2. All chemicals used were of analytical reagent grade. Solvents were distilled, kept under argon, and stored over activated molecular sieves. All catalysts were prepared without contact with air.

Catalyst Characterization

X-ray diffraction patterns of powders were collected at a step width of 0.02° and by counting 10 s at each step in the 2θ range of interest using a Siemens D-500 X-ray diffractometer equipped with a graphite monochromator and a Cu target.

Samples for TEM studies were suspended in methanol, in an ultrasonic bath, to form slightly turbid suspensions. A drop of the suspensions was deposited on carbon-coated copper grids, where the alcohol evaporated leaving films of catalyst particles. EDX measurements were carried out in STEM mode using a Hitachi H 800-MT transmission electron microscope operating at 175 keV with a Kevex 8000 Quantum System. The X-rays emitted upon electron irradiation were acquired in the range 0–10 keV. Electron diffraction studies were conducted with a Hitachi H 800-NA transmission electron microscope operating at 200 keV in convergent beam mode (CBED) with a 2–5 nm probe.

X-ray photoelectron spectra were acquired with a Fisons ESCALAB 200R spectrometer equipped with a hemispherical electron analyzer and a Mg$K\alpha$ 120 W X-ray source. The powder samples were pressed into small aluminum cylinders and then mounted on a sample rod placed in a pretreatment chamber and outgassed at ambient temperature. Subsequently they were re-reduced *in situ* by hydrogen at 673 K for 1 h, and after cooling to ambient temperature they were moved into the analysis chamber. The pressure in the ion-pumped analysis chamber was below 3×10^{-9} Torr ($1\ \text{Torr} = 133.33\ \text{N m}^{-2}$) during data acquisition. The intensities were estimated by calculating the integral of each peak after smoothing and subtraction of the "S-shaped" background and fitting the experimental curve to Lorentzian and Gaussian lines of variable proportion. Each spectral region was signal-averaged for 60 to 250, depending on the peak intensity, in order to improve the signal-to-noise ratio. Binding energies (BE) were referred to the adventitious C 1s line at 284.9 eV. This reference gave BE values with an accuracy of ±0.2 eV.

Catalytic Activity

n-Hexane conversion was carried out in a continuous flow glass microreactor at atmospheric pressure. A feed of hydrogen saturated with *n*-hexane vapor was generated by bubbling hydrogen (20 ml min^{-1}) through a thermostatted saturator maintained at 298 K. The H_2/*n*-hexane molar ratio was circa 4. The purity of *n*-hexane was at least 99%; 30–80 mg of catalyst was used for each of the reaction tests and diluted with inactive SiC, giving a catalyst bed volume of 0.5 ml.

All catalysts used in this study were re-reduced *in situ* prior to the reaction at 673 K for 1 h in flowing hydrogen. After the reduction treatment, the reactor temperature was lowered to 453 K in flowing hydrogen and the catalyst was aged by increasing the temperature from 453 to 753 K (5 K min^{-1}) under the reaction mixture of hydrogen and *n*-hexane. At 753 K the reactor effluent was sampled on line every 75 min for circa 20 h. Products were separated in a TRB-1 capillary column (100-m long, 0.25 i.d.) and a Hayesep column (6-m long, 2.16-mm i.d.), coupled to a flame ionization detector and a thermal conductivity detector, respectively, on a 3400 VARIAN gas chromatograph equipped with an automated gas sample valve. Under our experimental conditions, no dimethylbutanes, cyclohexadienes, methylcyclopentenes, or methylcyclopentadienes were obtained in appreciable amounts. Response factors and retention times were calibrated using appropriate standards. When 3-hexenes were detected they were not quantified due to their low yield and proximity to *n*-hexane peak.

RESULTS AND DISCUSSION

Characterization of Catalysts

The catalysts prepared were Pt/SiO_2, $5Pt1Sn/SiO_2$, $2Pt1Sn/SiO_2$, $1Pt1Sn/SiO_2$, $1Pt2Sn/SiO_2$, and $1Pt5Sn/SiO_2$. They were characterized by XRD, TEM, ED, EDX, and XPS techniques. The Pt/SiO_2 catalyst showed well-dispersed platinum particles (1.8 nm size) and the $1Pt1Sn/SiO_2$ catalyst showed a single well-defined PtSn alloy supported on silica as reported previously (13).

In Fig. 1 XRD patterns of the $aPtbSn/SiO_2$ catalysts are shown. When $a \geq b$ only the PtSn phase was found by this technique, the diffraction peaks being more intense as the a/b ratio approached one. When $a < b$ other tin-rich metallic phases were found. The XRD pattern of the $1Pt2Sn/SiO_2$ catalyst showed the presence of PtSn and $PtSn_2$ alloys, and the $1Pt5Sn/SiO_2$ catalyst had an XRD pattern assigned to $PtSn_2$ and metallic Sn.

Transmission electron microscopy studies of the $aPtbSn/SiO_2$ catalysts with $a > b$ showed hexagonal particles of PtSn alloy with a platelet morphology and Pt particles highly dispersed on silica, more abundant for higher a/b ratios. The mono- or bimetallic nature of these particles was confirmed by EDX, and their structure was examined by electron nanodiffraction. Figure 2 shows a representative transmission electron micrograph which corresponds to the

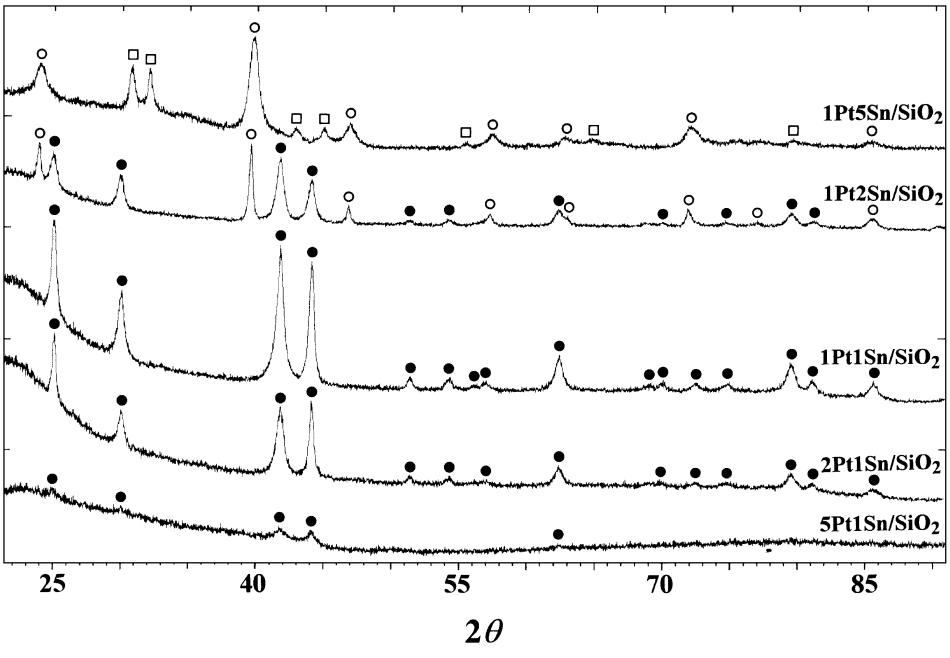

FIG. 1. XRD patterns of the *a*Pt*b*Sn/SiO_2 catalyst: ●, PtSn; ◯, $PtSn_2$; □, Sn.

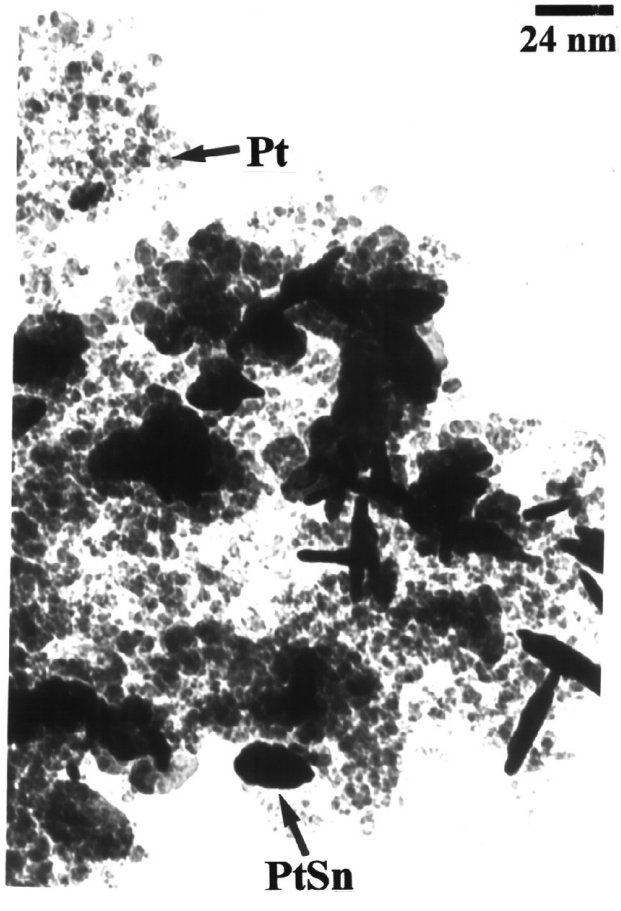

FIG. 2. Bright field TEM image of 2Pt1Sn/SiO_2 catalyst. Both Pt and PtSn particles are present.

2Pt1Sn/SiO_2 catalysts, where both Pt and PtSn particles are present. In Fig. 3 representative EDX analyses of individual Pt and PtSn particles are shown. Electron nanodiffraction patterns of some of the PtSn particles showed in all cases, after a careful indexation, the (hcp) PtSn alloy structure (Fig. 4).

Transmission electron microscopy studies of the *a*Pt*b*Sn/SiO_2 catalysts with $a < b$ showed the presence of PtSn, $PtSn_2$, and Sn metallic phases. For the 1Pt2Sn/SiO_2 catalyst only PtSn and $PtSn_2$ particles were found, whereas for the 1Pt5Sn/SiO_2 catalyst tin particles were also detected. In Fig. 5 a representative transmission electron micrograph corresponding to the catalyst 1Pt2Sn/SiO_2 is shown. EDX patterns of PtSn and $PtSn_2$ particles were consistent with their bimetallic composition (Fig. 6). Electron nanodiffraction patterns of these particles corresponded to the hexagonal PtSn or the cubic $PtSn_2$ alloy structure. The electron nanodifraction pattern obtained for an individual $PtSn_2$ particle in the 1Pt2Sn/SiO_2 catalyst is shown in Fig. 7.

In Fig. 8 the particle size distributions obtained from TEM for the different phases in the *a*Pt*b*Sn/SiO_2 catalysts are depicted. In each case more than 200 particles were used. It is remarkable that each observed phase has a similar particle size distribution in all catalysts prepared. It appears that the Pt/Sn ratio determines the stoichiometry of the $PtSn_x$ alloy formed, although the crystal size of the resulting alloy does not depend upon this ratio.

The Si 2p, Pt 4f, Sn 3d, and Cl 2p core level spectra were recorded for all the samples. The absence of any photoemission in the energy region of Cl $2p_{3/2}$ photoelectron indicated complete removal of chlorine during thermal treatments.

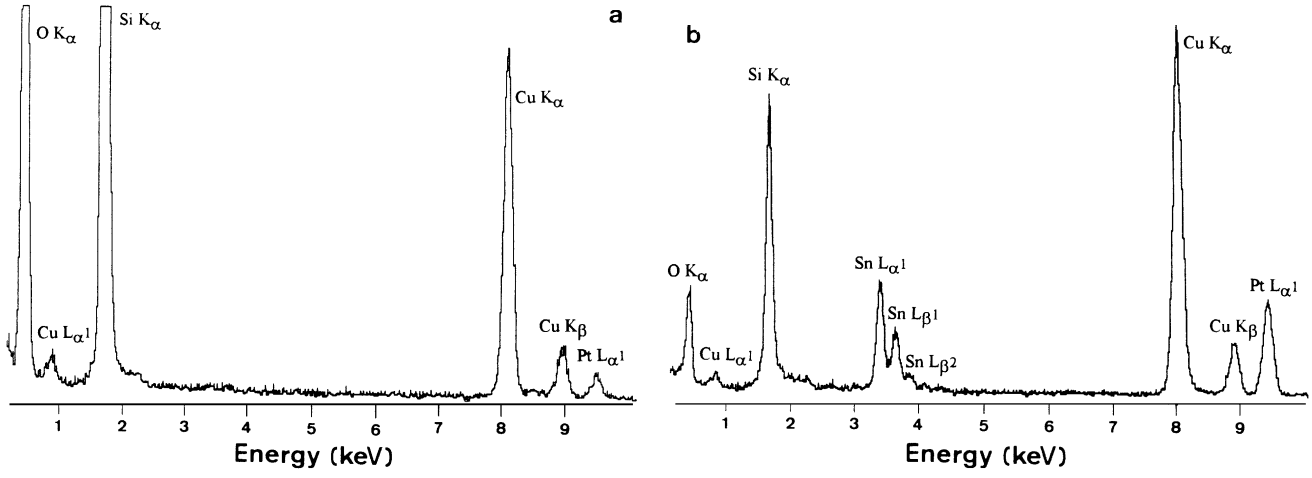

FIG. 3. EDX patterns of representative Pt (a) and PtSn (b) particles of the 2Pt1Sn/SiO_2 catalyst.

This was also confirmed by chemical analysis. A single component in the Pt 4f peak was observed for all the catalysts. The BE of the most intense Pt $4f_{7/2}$ peak located at 71.2–71.5 eV (Table 1) confirms that platinum was completely reduced to Pt^0. It is emphasized that differences in the BEs of Pt in metallic state and in alloy compounds are very small. The Sn 3d profiles were complex. By applying curve synthesis procedures to the experimental Sn 3d profiles, two tin components at 484.6–485.0 and 487.2–487.5 eV, assigned to Sn^0 and Sn^{2+}, respectively, have been obtained (Table 1).

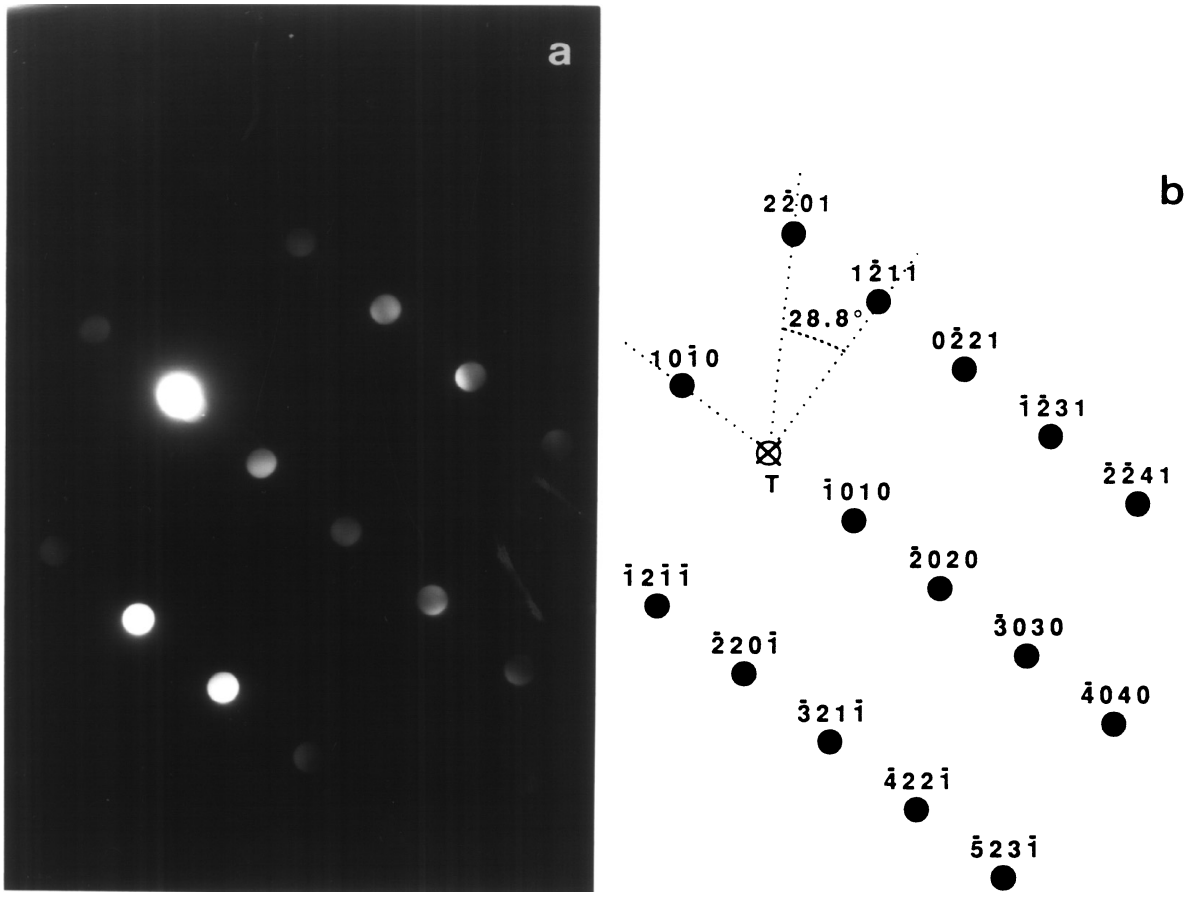

FIG. 4. (a) Electron nanodifraction pattern of a representative hexagonal particle of the 2Pt1Sn/SiO_2 catalyst, the particle has the PtSn (hcp) structure oriented in the [1$\bar{2}$16] crystallographic direction. (b) Indexed nanodiffraction pattern shown in (a).

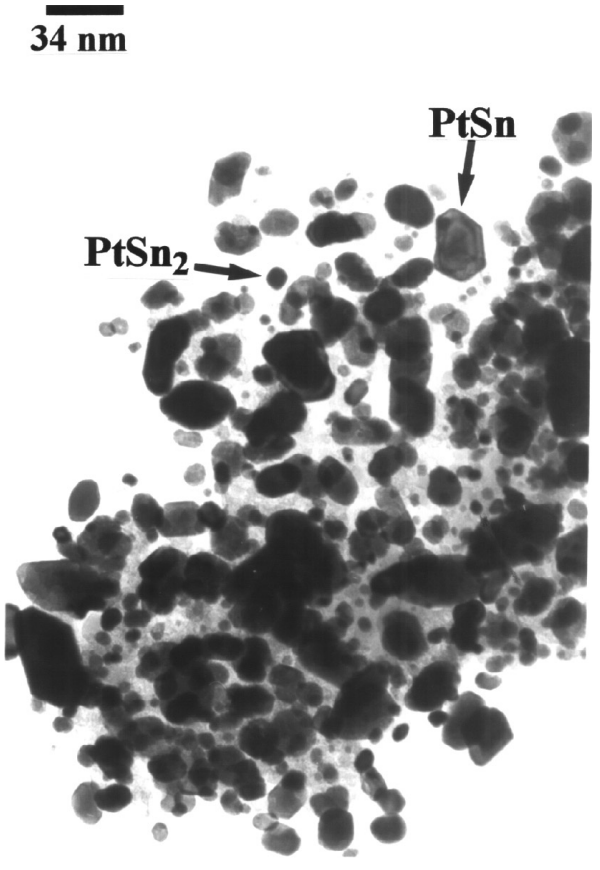

FIG. 5. Bright field TEM image of 1Pt2Sn/SiO_2 catalyst. Both PtSn and $PtSn_2$ particles are present.

The Sn^0/Sn_{total} ratio, which represents the ratio of the area of Sn^0 component to the total area of the Sn 3d peak, is also listed in Table 1. This Sn^0/Sn_{total} ratio was greater than 0.5 for all catalysts except 1Pt2Sn/SiO_2, in which the PtSn and $PtSn_2$ phases were shown by TEM, EDX, and electron nanodiffraction; the remaining Sn was probably oxidized. The Pt/Sn atomic ratios on the surface, which were calculated from XP spectra and sensitivity factors according to Wagner *et al.* (15) are also shown in Table 1. The *a*Pt*b*Sn/SiO_2 catalysts with $a < b$ showed low surface Pt/Sn ratios, indicating a high segregation of Sn on the surface. Differences between XPS results and the surface composition expected for the metallic phases characterized by the bulk techniques may indicate a heterogeneous nature of the surface of these catalysts.

TABLE 1

Binding Energies (eV) of Core Electrons and XPS Atomic Ratios for *a*Pt*b*Sn/SiO_2 Catalysts

Catalyst	Pt $4f_{7/2}$	Sn $3d_{5/2}$	Sn(0)/Sn (%)	Pt/Sn
Pt/SiO_2	71.3	—	—	—
5Pt1Sn/SiO_2	71.5	484.7 487.2	71	1.73
2Pt1Sn/SiO_2	71.4	484.6 487.3	77	0.86
1Pt1Sn/SiO_2	71.2	484.7 487.5	60	1.10
1Pt2Sn/SiO_2	71.2	484.9 487.2	39	0.11
1Pt5Sn/SiO_2	71.2	485.0 487.4	58	0.31

Catalytic Activity

For all catalysts the transformation of *n*-hexane was followed for 18–22 h after an accelerated aging treatment as indicated in the experimental section. Figure 9 shows the evolution of the deactivation percentage calculated from the ratio [(initial activity-activity(t))/initial activity] with the time (t) on stream for Pt/SiO_2 and *a*Pt*b*Sn/SiO_2 catalysts

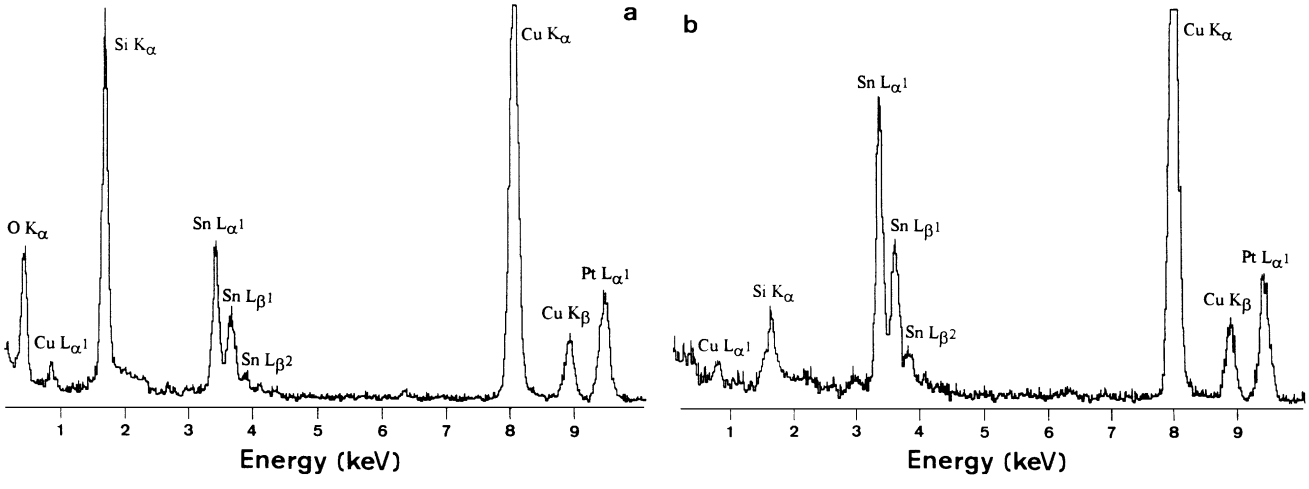

FIG. 6. EDX patterns of representative PtSn (a) and $PtSn_2$ (b) particles of the 1Pt2Sn/SiO_2 catalyst.

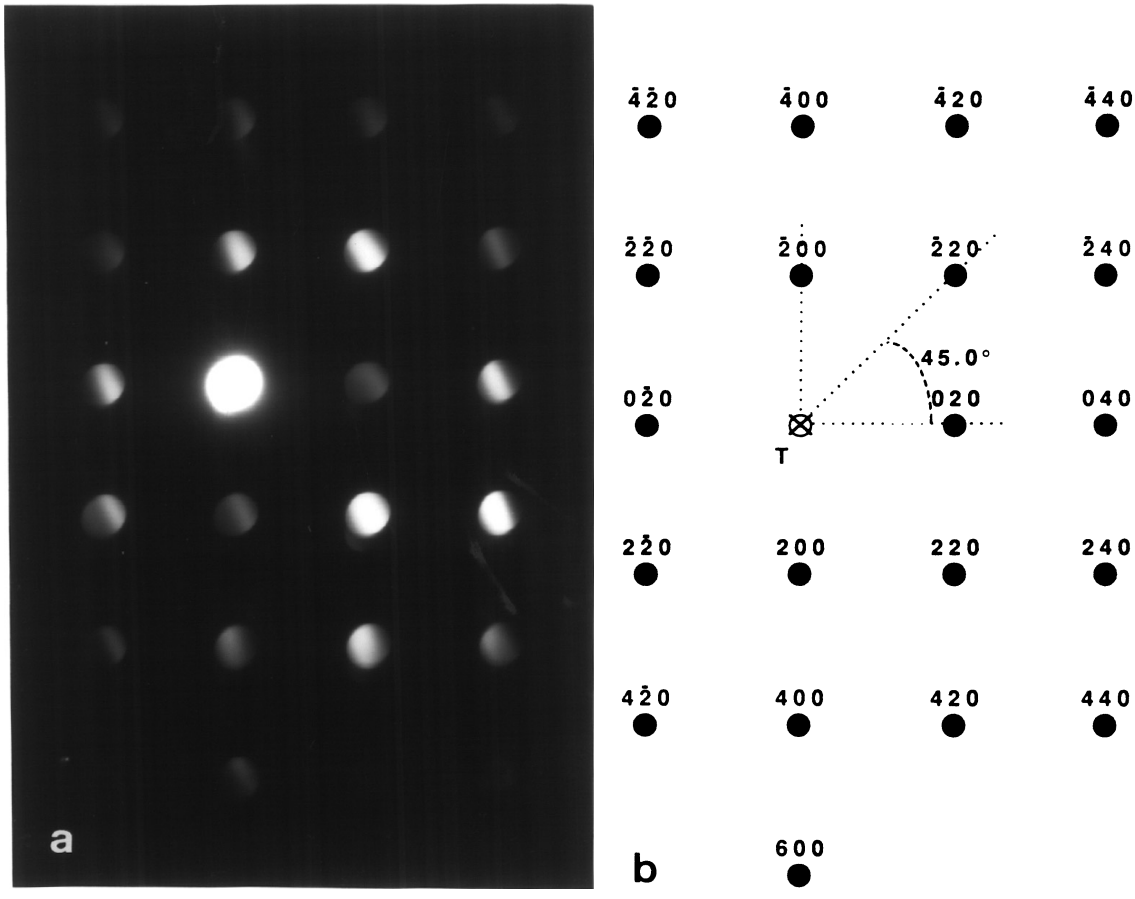

FIG. 7. (a) Electron nanodiffraction pattern of a representative cubic particle of the 1Pt2Sn/SiO_2 catalyst. The particle has the $PtSn_2$ structure oriented in the [100] crystallographic direction. (b) Indexed nanodiffraction pattern shown in (a).

with $a \geq b$. For catalysts with $a > b$ the deactivation percentage was a logarithmic function of time. The catalyst 1Pt1Sn/SiO_2 showed a negligible deactivation over time under these conditions (Fig. 9). This catalyst was also studied in the absence of previous accelerated-aging treatment for 4 h under reaction and a negligible deactivation over time was also shown in this case.

As mentioned above, for those catalysts with only silica-supported Pt or Pt and PtSn phases, the extent of PtSn alloy formation increases with a/b decreasing from 5 to 1. From this and Fig. 9 it could be inferred that the presence of PtSn alloy decreased the deactivation process. The lower the deactivation the greater the extent of PtSn alloy formation.

Taking into account the particle size of Pt and PtSn phases in these catalysts (see Fig. 8) it can also be inferred that PtSn alloy is much more active per surface platinum atom than supported platinum catalyst.

Table 2 shows the analysis of reaction products for these catalysts after time on stream between 1 and 3 h under differential conditions (conversion ca 13%).

The presence of PtSn phase increased the dehydrogenation reaction and decreased the benzene production and hydrogenolysis reaction. The 1Pt1Sn/SiO_2 catalyst, which had the only well-defined PtSn phase, mainly produced C_6 olefins and exhibited a lower activity for hydrogenolysis and benzene production (84.5% C_6 olefins, 3.3% hydrogenolysis, 2.2% benzene).

Our results show that benzene production decreased upon tin addition and PtSn alloy formation, and it was almost fully suppressed when only the PtSn alloy was present. The cyclohexene production showed the same trend. In contrast, the production of C_6 olefins increased continuously with the extent of PtSn formation, and reached a maximum for the 1Pt1Sn/SiO_2 catalyst, where all Pt and Sn were alloyed in the PtSn phase.

The catalytic behaviour of *a*Pt*b*Sn/SiO_2 catalysts with $b > a$ contrasts with those discussed above. They showed a fast linear deactivation up to circa 6 h and then they became inactive. The initial product distribution for these catalysts is given in Table 3; they present the highest selectivity to hydrogenolysis of all catalysts prepared. These catalysts also showed the highest concentration of oxidized tin species on the surface (see in Table 1 the Pt/Sn and Sn(0)/Sn ratios determined by XPS).

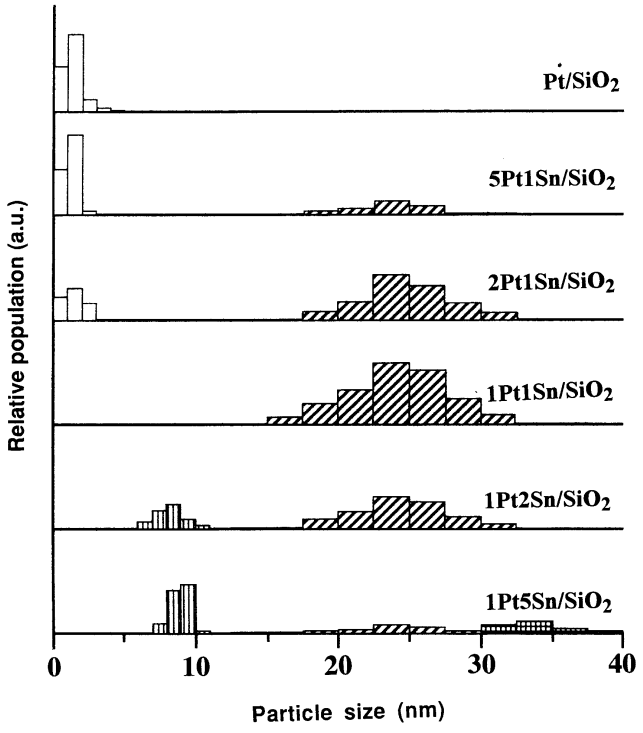

FIG. 8. Particle size distribution histograms obtained from TEM for the different phases in *a*Pt*b*Sn/SiO_2 catalysts: □, Pt; ▨, PtSn; ▥, $PtSn_2$; ▦, Sn.

The effect of Sn addition on Pt catalysts has been related to Pt–Sn interactions and consequently to the geometric and ligand effects produced by tin (12, 16–19).

To discuss these facts we can use the well defined characteristics of our catalysts. The platinum–tin alloy has an ordered structure in which the Pt and Sn atoms surround each other and a certain enrichment of the alloy surface with tin atoms is predicted by thermodynamics (20). This dilution of an active metal by an inactive one called "ensemble effect" is assumed to be responsible for drastic changes in selectivity in a given catalytic process.

In our case the catalyst 1Pt1Sn/SiO_2 is an almost perfect model for this situation. This sample only contains on surface the regular PtSn (hcp) alloy with a platelet morphology. We have found that the selectivity of this catalyst towards C_6 isomers, including methylpentanes and mainly C_6 olefins, is

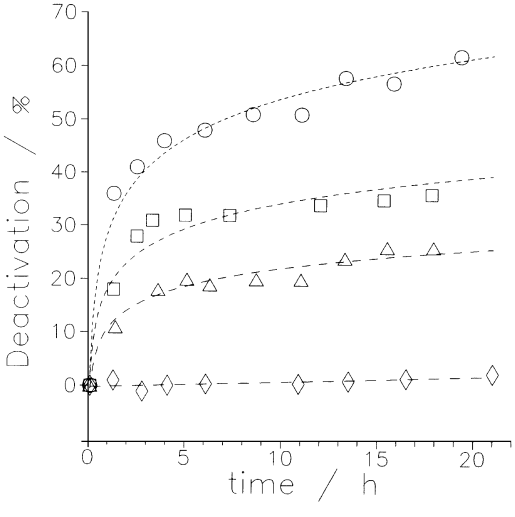

FIG. 9. Deactivation percentage as a function of reaction time for different catalysts: ○, Pt/SiO_2, initial activity value 1214 μmol · g^{-1} Pt · s^{-1}; □, 5Pt1Sn/SiO_2, initial activity value 484 μmol · g^{-1} Pt · s^{-1}; △, 2Pt1Sn/SiO_2, initial activity value 436 μmol · g^{-1} Pt · s^{-1}; ◇, 1Pt1Sn/SiO_2, initial activity value 189 μmol · g^{-1} Pt · s^{-1}.

TABLE 2

Product Distribution for the Reaction of *n*-Hexane over *a*Pt*b*Sn/SiO_2 ($a/b \geq 1$) Catalysts at 753 K ($H_2/C_6H_{14} = 4$, Total Conversion ca 13%)[a]

Catalyst	Pt/SiO_2	5Pt1Sn/SiO_2	2Pt1Sn/SiO_2	1Pt1Sn/SiO_2
C_1–C_5	8.8	7.8	11.7	3.3
C_6=[b]	35.4	53.5	64.9	84.5
2-mp	2.5	2.0	3.6	3.2
3-mp	3.7	1.7	2.8	5.3
mcp	8.9	2.3	2.2	0.9
ch	—	2.8	3.5	—
ch=	10.5	3.5	4.1	0.6
bz	30.2	26.4	7.2	2.2

[a] Abbreviations: 2-mp = 2-methylpentane; 3-mp = 3-methylpentane; mcp = methylcyclopentane; ch = cyclohexane; bz = benzene.

[b] Includes 1-hexene, *cis*-2-hexene, and *trans*-2-hexene. 3-hexene isomers were detected but not quantified due to their low yield and proximity to the *n*-hexane peak.

TABLE 3

Initial Product Distribution and Catalytic Activity for the Reaction of *n*-Hexane over *a*Pt*b*Sn/SiO_2 Catalysts with $b > a$ at 753 K ($H_2/C_6H_{14} = 4$)[a]

Catalyst	1Pt2Sn/SiO_2	1Pt5Sn/SiO_2
Conversion (%)	7.8	1.6
Activity (μmol · g^{-1} Pt · s^{-1})	121	23
C_1–C_5	24.3	99.8
C_6=[b]	67.6	—
2-mp	1.5	—
3-mp	2.3	—
mcp	2.7	—
ch	0.7	—
ch=	0.7	—
bz	0.2	0.2

[a] Abbreviations: 2-mp = 2-methylpentane; 3-mp = 3-methylpentane; mcp = methylcyclopentane; ch = cyclohexane; bz = benzene.

[b] Includes 1-hexene, *cis*-2-hexene, and *trans*-2-hexene.

over 90% and doubles that for Pt/SiO_2 catalyst. In fact, for the $aPtbSn/SiO_2$ catalysts with $a \geq b$ a continuous increase in the selectivity to C_6 olefins can be observed when increasing the extent of PtSn alloy formation from $5Pt1Sn/SiO_2$ to $1Pt1Sn/SiO_2$ (see Fig. 10). The isolated platinum atoms of supported PtSn alloy may be responsible for this behaviour since the catalytic dehydrogenation of chemisorbed reactants occurs on monoatomic Pt entities (21). Taking into account that these olefins are intermediates in aromatization, the lack of benzene would indicate easy desorption under these conditions, facilitated by tin through electronic and ensemble effects (18).

On the other hand, regarding the deactivation process, for silica-supported platinum catalysts the accumulation of carbonaceous species leads to the loss of platinum surface-area (22), meanwhile the higher stability of platinum–tin catalysts is related to Pt–Sn interactions (12). In our case the behaviour of $1Pt1Sn/SiO_2$ catalyst again strongly differs from the other catalysts. The self-poisoning process with carbonaceous residues formation could be regarded as a polymerization-type reaction of extensively dehydrogenated surface species. This process may be associated with contiguous Pt sites, $n > 3$ (23), this type of site is not available on the PtSn alloy, and the expected electron donation from tin to platinum would not favour hydrocarbon polymerization. The high performance of the $1Pt1Sn/SiO_2$ catalyst is thus strongly related to the presence of the unique homogeneously distributed PtSn alloy on surface. The negligible deactivation process observed on the well defined PtSn silica-supported alloy and their particular selectivity to dehydrogenated species may related to both ensemble and electronic effects.

The stability of the supported PtSn phase under reaction conditions was confirmed by TEM. Figure 11 shows a TEM micrograph of the $1Pt1Sn/SiO_2$ catalyst after reaction. Only PtSn particles can be seen, whose bimetallic composition was confirmed by EDX. An increase in particle size was observed after reaction, probably due to the reaction temperature, 753 K, slightly higher than reduction temperature (673 K).

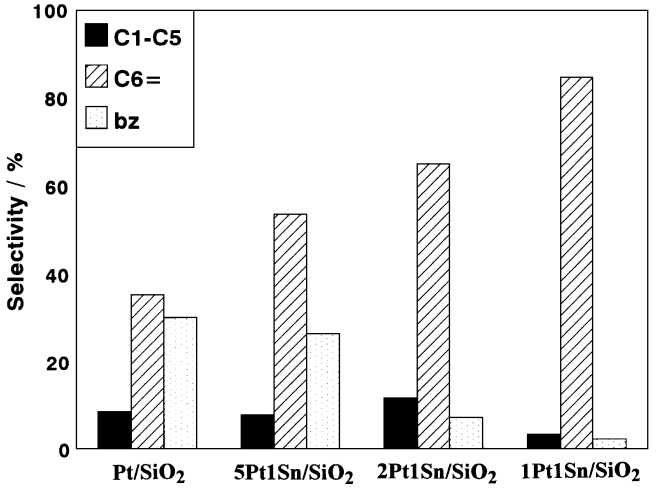

FIG. 10. Product distribution in the *n*-hexane skeletal reactions for $aPtbSn/SiO_2$ ($a \geq b$) catalysts.

FIG. 11. TEM micrograph of $1Pt1Sn/SiO_2$ catalyst after *n*-hexane hydroisomerization reaction at 753 K for 22 h.

CONCLUSIONS

Silica-supported platinum–tin catalysts with Pt : Sn molar ratios ranging from 5 : 1 to 1 : 5 have been prepared, and their behavior in the skeletal reactions of *n*-hexane has been studied. Among all the possible Pt_xSn_y phases (Pt, Pt_3Sn, PtSn, Pt_2Sn_3, $PtSn_2$, $PtSn_4$, Sn) (24), the preparation method only lead to some of them (which were characterized by XRD, TEM, ED, EDX, XPS): Pt and PtSn for catalysts with $Pt/Sn > 1$ molar ratio, PtSn for the catalyst with $Pt/Sn = 1$ molar ratio (13), and PtSn, $PtSn_2$, and Sn for catalysts with $Pt/Sn < 1$. For the catalysts with low Pt/Sn molar ratio, a segregation of Sn on surface was shown by XPS, and high selectivity to hydrogenolysis and fast deactivation process were observed. For the catalysts with $Pt/Sn \geq 1$ molar ratio, it was possible to relate their stability and selectivity to the presence of the PtSn phase on silica. Catalysts with

PtSn alloy were more stable and exhibited high selectivity to deshydrogenation reactions and low conversion to benzene and hydrogenolysis products.

ACKNOWLEDGMENTS

We thank DGICYT (MAT93-0477-C02 and MAT96-0859-C02) for financial support and the Serveis Científico–Tècnics UB for chemical analysis and apparatus facilities.

REFERENCES

1. Davis, B. H., *in* "Selectivity in Catalysis" (M. E. Davis and S. L. Suib, Eds.), ACS Symposium Series 517. Am. Chem. Soc., Washington, DC, 1993.
2. Coq, B., and Figueras, F., *J. Catal.* **85**, 197 (1984).
3. Li, Y. X., and Klabunde, K. J., *J. Catal.* **126**, 173 (1990).
4. Lei, Y. J., *Appl. Catal.* **72**, 33 (1991).
5. Margitfalvi, J. L., Jalett, H. P., Tálas, E., Baiker, A., and Blaser, H. U., *Catal. Lett.* **10**, 325 (1991).
6. Balakrishanan, K., and Schwank, J., *J. Catal.* **127**, 287 (1991).
7. Kappenstein, C., Saouabe, M., Guérin, M., Marecot, P., Uszkurat, I., and Paál, Z., *Catal. Lett.* **31**, 9 (1995).
8. Mériaudeau, P., Naccache, C., Thangaraj, A., Bianchi, C. L., Carli, R., Vishvanathan, V., and Narayanan, S., *J. Catal.* **154**, 345 (1995).
9. Margitfalvi, J. L., Hegedüs, M., and Tálas, E., *J. Mol. Catal.* **51**, 279 (1989).
10. Srinivasan, R., and Davis, B. H., *J. Mol. Catal.* **88**, 343 (1994).
11. Lin, L., Zang, J., Wu, R., Wang, C., and Du, H., *in* "Proceedings, 8th International Congress on Catalysis, 1984," Vol. IV, p. 565. Elsevier, Amsterdam, 1984.
12. Dautzenberg, F. M., Helle, J. N., Biloen, P., and Sachtler, W. M. H., *J. Catal.* **63**, 119 (1980).
13. Llorca, J., Ramirez de la Piscina, P., Fierro, J. L. G., Sales, J., and Homs, N., *J. Catal.* **156**, 139 (1995).
14. Cavinato, G., and Toniolo, L., *Inorg, Chim. Acta* **52**, 39 (1981).
15. Wagner, C. D., Davis, L. E., Zeller, M. V., Taylor, J. A., Raymond, R. H., and Gale, L. H., *Surf. Interface Anal.* **3**, 211 (1981).
16. Biloen, P., Helle, J. N., Verbeek, H., Dautzenberg, F. M., and Sachtler, W. M. H., *J. Catal.* **63**, 112 (1980).
17. Burch, R., and Garla, L. C., *J. Catal.* **71**, 360 (1981).
18. Shi, B., and Davis, B. H., *J. Catal.* **157**, 626 (1995).
19. Paál, Z., Dobrovolszky, M., Volter, J., and Lietz, G., *Appl. Catal.* **14**, 33 (1985).
20. Van Santen, R. A., and Sachtler, W. M. H., *J. Catal.* **33**, 202 (1974).
21. Biloen, P., Dautzenberg, F. M., and Sachtler, W. M. H., *J. Catal.* **50**, 77 (1977).
22. Sharma, S. B., Ouraipryvan, P., Nair, H. A., Balaraman, P., Root, T. W., and Dumesic, J. A., *J. Catal.* **150**, 234 (1994).
23. Clarke, J. K. A., *Chem. Rev.* **75**, 291 (1975).
24. Hansen M., "Constitution of Binary Alloys," p. 1142. Mc Graw–Hill, New York, 1958.